ELASTOPLASTIC STRUCTURAL ANALYSIS OF THE PADERNO D'ADDA BRIDGE (ITALY, 1889) BASED ON LIMIT ANALYSIS

Ferrari Rosalba[1]*, Cocchetti Giuseppe*[2]*, Rizzi Egidio*[3]

ABSTRACT

The Paderno d'Adda bridge is a marvellous historical iron arch bridge that was built in 1889. It allows connecting the provinces of Lecco and Bergamo across the Adda river, between Paderno d'Adda and Calusco d'Adda, near Milano, northern Italy. The bridge was designed for railway needs and its use is two-fold: a railway track is located in the inner deck of the upper continuous beam; automotive traffic runs on top of it. Today, after 123 years of continuous duty, the viaduct is still in service, with trains crossing at slow speed and alternated one-way road traffic restricted to no heavy-weight vehicles. Despite these duties, the bridge seems to have suffered from limited maintenance. With the final purpose of elaborating a safety assessment of the structure, an inelastic structural analysis of the viaduct is performed, based on a finite element model that takes into account a perfect elastoplastic behaviour of the various structural members and is apt to comply with typical principles of Limit Analysis. Specifically, the critical load multiplier and relevant collapse mode are investigated, for different static loading conditions on the bridge. Also, the characteristic non-linear load/displacement response curves of the bridge are traced by incremental analyses up to the true limit load and the various critical members of the structure are identified. A further intention of this work consists in promoting interest at the international level on the Paderno d'Adda bridge, as a beautiful, living industrial monument of the scientific and technological developments of that time, by referring particularly to its present and future destinations.

Keywords: *Historical iron arch bridge, Non-linear FEM model, Elastoplastic structural analysis, Limit Analysis, Collapse load multiplier, Collapse mode*

1.   INTRODUCTION

The Paderno d'Adda bridge is a beautiful iron viaduct built in 1889 by the *Società Nazionale delle Officine di Savigliano (SNOS)*, in response to needs from rapidly-growing industrial activities in Lombardia towards the end of 1800 [1,2]. Specifically, within the expansion of the local railway network, it became necessary to acquire an elevated crossing on the river Adda, North-East from Milano. The remarkable structural concept elaborated for the bridge by designer Jules Röthlisberger (1851-1911), head of the SNOS Technical Office since 1885, was that of raising a stiff but slender symmetric doubly built-in parabolic arch among the two banks of Paderno d'Adda (right bank) and Calusco d'Adda (left bank), of about 150 m of horizontal span and 37.5 m of vertical rise, supporting then, together with vertical truncated pyramidal piers, a straight upper box continuous beam on nine bearings of 266 m of length [1, 2] (Fig. 1).

---

[1] Doctoral Student, Università di Bergamo, Facoltà di Ingegneria (Dalmine), Dipartimento di Progettazione e Tecnologie, viale G. Marconi 5, I-24044 Dalmine (BG), Italy, rosalba.ferrari@unibg.it

[2] Associate Professor, Università di Bergamo, Facoltà di Ingegneria (Dalmine), Dipartimento di Progettazione e Tecnologie, viale G. Marconi 5, I-24044 Dalmine (BG), Italy, Politecnico di Milano, Dipartimento di Ingegneria Strutturale, piazza L. da Vinci 32, I-20133 Milano, Italy, giuseppe.cocchetti@unibg.it

[3] Professor, Università di Bergamo, Facoltà di Ingegneria (Dalmine), Dipartimento di Progettazione e Tecnologie, viale G. Marconi 5, I-24044 Dalmine (BG), Italy, Corresponding Author, egidio.rizzi@unibg.it

Fig. 1 Present up-stream view of the iron arch bridge (1889) from Paderno d'Adda (right bank)

The bridge probably represents one of the very first large structures designed through a practical application of the so-called *"Theory of the Ellipse of Elasticity"*, a graphical-analytical method of structural analysis that was developed in the wake of *Graphic Statics*, specifically at the Polytechnical School of Zürich (where Röthlisberger was formed) by Karl Culmann (1821-1881) and by his pupil Wilhelm Ritter (1847-1906). A specific account on that has been provided in Laurea Thesis [3] and in previous *SAHC08* paper [4], which has opened-up the way to a modelling study on the bridge at the University of Bergamo, by a research project that was started in 2005 [3-10]. This has led to the assembly of a complete linear FEM model of the structure, within a commercial FEM program (*ABAQUS*), as further refined here by an independent non-linear implementation (*MATLAB*) in an elastoplastic setting.

The bridge was built with a wrought iron material, with riveted joints. According to the original SNOS Report [1], about 2600 tons of metals were employed in the construction. Details on the various characteristic features of the bridge are available in [2] and have been analysed and further reported in [3-10]. Along its history, the Paderno d'Adda bridge has undergone a few modifications and repairs. Despite its continuous duties, only two documented systematic static try-out loading tests with added load seem to have been carried-out, in 1889 and 1892, in order to compare as well the outcomes of theoretical predictions elaborated by the SNOS at design stage.

Successful direct comparisons to such try-out evidences have been achieved in the research project above [3-10], by producing static results through a linear FEM model loyal to design-stage conditions, as documented by the original technical drawings that have been accessed at the *Archivio Nazionale di Torino* (see extensive description in [10]). Specifically, linear structural simulations in previous *SAHC10* paper [8] have shown full consistency among FEM predictions and expected/recorded SNOS data. Further, a first modelling investigation on the dynamic characteristics of the bridge has been attempted in [9], in terms of the determination of the main mode frequencies and associated mode shapes, with results that appeared to be consistent to those from preliminary field investigations and dynamic identification on the bridge, based on ambient vibration tests that have been carried-out recently by colleagues at Politecnico di Milano [11-12]. This has led to the development of a permanent monitoring system of the bridge, that is being now put in place by them [13], as conceived to assess possible degradation of structural performance. Further in light of this, the completion of a reliable FEM model of the viaduct appears to be truly fundamental for a comprehensive understanding of the structural performance of the bridge, which in the end should properly address the present morphology and state of conservation of the structure.

Based on such previous know-how, the present research study has been developed in the direction of modelling the global non-linear elastoplastic behaviour of the bridge. Reference is still made so far to the characteristics at design stage; the hypothesis of perfect elastoplastic behaviour with unlimited ductility of all the structural members has been assumed. In particular, focus is made here on the determination of the collapse load multiplier and relevant collapse mechanism, for various static try-out railway loading conditions on the bridge. The characteristic load/displacement curves are traced by incremental analyses up to the true limit load and the critical members in the various parts of the structure are identified.

The non-linear structural analyses have been performed with an elastoplastic FEM formulation that has been implemented in an autonomous computer code, running within a *MATLAB* environment. Details on the adopted computational formulation strategy and its code implementation are going to be

2172

provided elsewhere [14]; a brief account on that is reported in Section 2, with basic description of the adopted FEM formulation. The morphological and geometrical features of the structure have been exported from the previous FEM model implemented in a commercial FEM code (*ABAQUS*). This has been built by assembling a true 3D truss frame with beam elements, mutually connected at the nodes, as composed of three main structural parts: bearing doubly-built-in parabolic arch, vertical piers, upper box continuous beam. Details on the different parts and total assembly of the pre-existing FEM model of the bridge, imposed boundary conditions and considered loading cases are available in [3-10]. The final assembly of the complete truss FEM model of the Paderno d'Adda bridge collects 5337 beam elements, 2216 structural nodes and 13296 degrees of freedom (nodal displacements and rotations). The material properties adopted in the FEM model are taken as representative of a wrought iron material [1,2]: specific weight $\gamma = 7.7$ t/m^3; Young's modulus $E = 17000000$ t/m^2; Poisson's ratio $v = 0.3$; corresponding shear modulus $G = 6540000$ t/m^2; yield stresses $\sigma_y = 6.00$ kg/mm^2 and $\tau_y = \sigma_y/\sqrt{3} = 3.46$ kg/mm^2.

2. NON-LINEAR ELASTOPLASTIC FEM FORMULATION

The salient characteristic features of the non-linear elastoplastic FEM formulation are briefly resumed below, with reference to the implementation of the perfect elastoplastic behaviour of the structural members. General characteristics of the algorithm formulation are rooted in [15]; detailed information on the present computational implementation is going to be provided elsewhere [14]. The FEM formulation is based on a classical Euler-Bernoulli beam finite element, according to the following peculiar hypotheses: straight elements, uniform cross section, homogeneous material properties, transverse displacements modelled by cubic shape functions (i.e. negligible shear strain effects are considered), axial displacements and rotations varying linearly along the beam element.

Plastic deformation has been concentrated at the element edges, *A, B* (a schematic 2D representation is depicted in Fig. 2), where two plastic joints (as a generalization of the classical plastic hinge concept in the Limit Analysis of frames, see e.g. [15] and references quoted therein) have been inserted. In each plastic joint, the assumed generalized kinematic variables are two relative plastic rotations (each around a principal axis of the cross section – labels 1,2), an axial elongation and a relative rotation around the beam axis. Specifically, axial elongation and axial rotation are (possibly) activated in only one of the two joints (*A* or *B*), in order to avoid unrealistic free rigid body movements; then, only 6 internal kinematic variables are required for each beam element. Shear effects have not been considered so far.

Fig. 2 Schematic representation of a beam finite element with plastic joints (at edges A and B)

For each 3D beam finite element, a linear rate relation can be obtained between the increments of: the 12 static actions at the extremes of the beam element ($\dot{\mathbf{h}}$), the corresponding 12 nodal displacements and rotations ($\dot{\mathbf{u}}$), the above-mentioned 6 generalized kinematic plastic variables ($\dot{\boldsymbol{\eta}}$). Namely (see [15]):

$$\dot{\mathbf{h}} = \mathbf{k}\dot{\mathbf{u}} + \mathbf{d}\dot{\boldsymbol{\eta}} \tag{1}$$

where **k** is the classical 12 × 12 elastic stiffness matrix of the finite element and **d** is an additional 12×6 plastic stiffness matrix.

The irreversible behaviour of the plastic joints is described by an associative, perfectly-plastic, generalized variable model, in terms of 7 of the 12 static variables, namely normal action, principal bending moments at extremes *A, B*, and constant twisting moment, as defined below. As a simplifying assumption, a piece-wise linear, uncoupled elastoplastic behaviour is adopted in terms of such internal static variables, namely a Rankine-type boxed-form yield domain is assumed in the space of static variables.

The analytical description of the interaction domain for the beam element is then stated in terms of the following inequalities:

$$\begin{cases} N^- \leq \min\left(N^A, N^B\right) \leq \max\left(N^A, N^B\right) \leq N^+ \\ M_t^- \leq M_t \leq M_t^+ \\ M_1^- \leq M_1^A \leq M_1^+, \qquad M_2^- \leq M_2^A \leq M_2^+ \\ M_1^- \leq M_1^B \leq M_1^+, \qquad M_2^- \leq M_2^B \leq M_2^+ \end{cases} \tag{2}$$

where N is the axial force, M_t is the torque (uniform along the beam), M_1 and M_2 are the bending moments with respect to the two principal axes of inertia of the cross section (indexes A and B refer again to the beam edges, Fig. 2). Yield limits $N^-, N^+, M_t^-, M_t^+, M_{1,2}^-, M_{1,2}^+$ are taken constant and obtained from material yield limits (σ_y, τ_y) and cross section geometrical characteristics as:

$$N^+ = -N^- = A\sigma_y, \quad M_{1,2}^+ = -M_{1,2}^- = \alpha M_{1,2}^e = \alpha(2J_{1,2}/h_{1,2})\sigma_y, \quad M_t^+ = -M_t^- = \beta M_t^e = \beta(J_t/b)\tau_y \tag{3}$$

where α and β are bending and torsion section shape factors (taken here as $\alpha = 1.1$ and $\beta = 1.5$ for all the elements) and $J_{1,2}$, J_t, $h_{1,2}$, b are flexural principal inertias, torsional inertia, principal heights and characteristic profile thickness of the cross section.

When some of the yield modes are active in the current time interval of the integration process (say, for instance, $\max(N^A, N^B) = N^+$ and $M_1^A = M_1^+$), the increment of each associated internal action is set to zero and the corresponding incremental relations in Eq. (1) can be solved for the increments of the corresponding activated kinematic internal variables ($\dot{\boldsymbol{\eta}}'$) as (linear) functions of the displacement increments ($\dot{\mathbf{u}}$):

$$\dot{\mathbf{h}}' = \mathbf{k}'\dot{\mathbf{u}} + \mathbf{d}'\dot{\boldsymbol{\eta}}' = \mathbf{0} \quad \Rightarrow \quad \dot{\boldsymbol{\eta}}' = (-\mathbf{d}'^{-1}\,\mathbf{k}')\,\dot{\mathbf{u}} \tag{4}$$

Finally, by substituting into Eq. (1) the second expression in Eq. (4), a direct force/displacement incremental relationship, governed by a symmetric elastoplastic stiffness matrix ($\mathbf{k}_{ep}$) can be obtained for the generic beam finite element:

$$\dot{\mathbf{h}} = \mathbf{k}_{ep}\,\dot{\mathbf{u}} \tag{5}$$

The global structural (linear) solving rate system is obtained by the assembly of the elastoplastic matrices of each finite element and of the equivalent nodal force vector increment:

$$\mathbf{K}_{ep}\,\dot{\mathbf{U}} = \dot{\mathbf{F}} \tag{6}$$

where $\mathbf{U}$ is the vector collecting the (un-constrained) degrees of freedom of the whole structure, $\mathbf{F}$ is the nodal force vector coming from the given applied forces and $\mathbf{K}_{ep}$ is the global tangent stiffness matrix of the structure.

Being this last relationship of a linear kind, the whole time integration process can be split into a sequence of time intervals in which all static and kinematic quantities vary linearly along each step (see e.g. [15]). A scalar multiplier factor λ is considered as a load amplifier common to a set of basic (live) loads. The internal kinematic variables, active along the time interval, are selected according to the active yield planes at its beginning, Eq. (4); however, if the computed incremental solution that can be extracted from Eq. (6) would imply negative dissipation for any of the active modes (for instance, if a tensile yielding axial force acts in a beam and, instead, a length shortening would be obtained in the incremental solution), then that active mode is actually deactivated, the stiffness matrix is newly updated and the incremental solution is re-computed. On the other hand, when an active mode has been deactivated at the beginning of the time increment and the incremental solution would render an increment of the static action corresponding to that mode, producing thus a violation of the perfectly-plastic yield condition (for instance, an axial force becoming higher than the yield limit at the end of the time increment), this would mean that such a mode shall be included among the active ones, from the beginning of the time interval; then, the stiffness matrix has to be updated before the new

computation of the incremental solution. Once all conditions of non-negative dissipation and perfectly-plastic yielding described above are fulfilled, the algorithm calculates, among all non-activated modes, the load multipliers leading to all new possible activations. The minimum among such estimated multipliers is set as the true value of λ at the end of the increment. Then, the corresponding increments of static $\dot{\mathbf{h}}$ and kinematic $\dot{\mathbf{u}}$ quantities (internal actions and displacements) are updated proportionally, from the original incremental solution. In this sense, the piece-wise linear elastoplastic response of the structure to proportionally-increasing external actions can be computed "exactly", in the spirit of Limit Analysis. In the structural solution, boundary conditions are imposed with "ad-hoc" procedures [14].

Finally, the collapse of the structure is reached when the minimum eigenvalue of the global (updated) tangent stiffness matrix $\mathbf{K}_{ep}$ vanishes (with numerical tolerances in the order of 10^{-15}) and the corresponding eigenvector leads to a positive incremental dissipation for each active mode.

3. ELASTOPLASTIC RESULTS AND ENGINEERING IMPLICATIONS

Though the present FEM model has been conceived so far at design stage, the current perfect elastoplastic structural analysis provides crucial information about the ideal load-carrying capacity of the bridge under limit service conditions. As previously presented for the elastic analyses in [8-10], accidental loading conditions associated to four static try-out tests performed by the SNOS [1,2] are considered. These tests (Fig. 3) took place on 12-19 May 1889, and were carried-out using six locomotives with tender, each of 83 t of weight, corresponding to a uniformly-distributed load on the beam of $q = 5.1$ t/m. Loads have been applied here to the nodes of the FEM model at the railway level. In Fig. 3 the total load applied to the structure is reported for each test, which is obtained as $Q = n\, q\, l$, where l is the length of each span of the upper continuous beam ($l = 33.25$ m) and n is the number of loaded spans, according to the load distributions in Fig. 3 ($n = 2$ or 3). Self-weight is pre-loaded on the bridge (through specific weight γ), leading to elastic deformations, before starting the incremental elastoplastic analyses, which develop at increasing accidental load. Salient results are presented as follows (Figs. 4-9, Table 1). All following representations have been generated after running the analyses, by appropriate post-processing of the stored data.
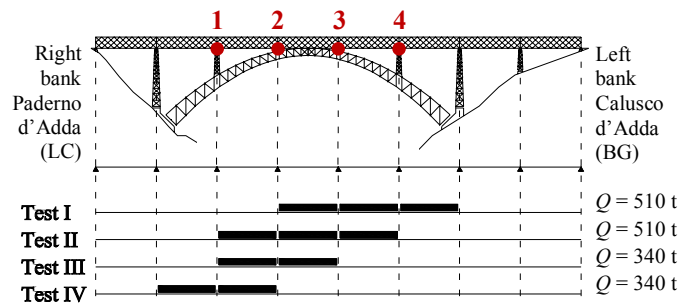

Fig. 3 Scheme of considered four static try-out configurations (view from down-stream), with value of total load applied to the structure for each test and indication of four control points (red circles)

First, for each of the four try-out loading configurations in Fig. 3, the deformed configuration of the bridge at incipient collapse with amplification factor set to 100 (Figs. 4-7a), the characteristic non-linear load/displacement response curve (Figs. 4-7b) and the localisation of the plasticised members have been reported (Figs. 4-7c). The response plots in Figs. 4-7b show the computed step-by-step evolutive solutions, with reference to values read at the beginning of each time interval. In particular, the horizontal axis depicts the vertical displacement (Δ) of the node that, in the end, has shown the maximum displacement at incipient collapse; the vertical axis reports the amplified accidental load $P = \lambda\, Q$, where λ is the load multiplier related to the incremental solution of the non-linear elastoplastic analysis (Section 2). Notice that in the plots in Figs. 4-7b, the non-zero initial displacement (at $P = 0$) is due to self-weight only, namely to a pre-imposed permanent load not affected by the load multiplier (i.e. load multiplier λ affects just the accidental load linked to the locomotive distributions). Moreover, for each loading case, the end point of the P-Δ curve refers to the so-estimated collapse of the structure in terms of vanishing minimum eigenvalue of the tangent stiffness matrix of the structure (Section 2). Figs. 4-7c show a plasticity map of plastic activations in

the various structural members at increasing load multiplier λ. It scores the plastic modes that are activated at the beginning of each time increment. Each marker represents one activated mode in the structure, as described below. On the two lines, the activation of axial (N) and bending modes (M) are shown, respectively. Notice that no torsional modes have been activated during the analyses, which
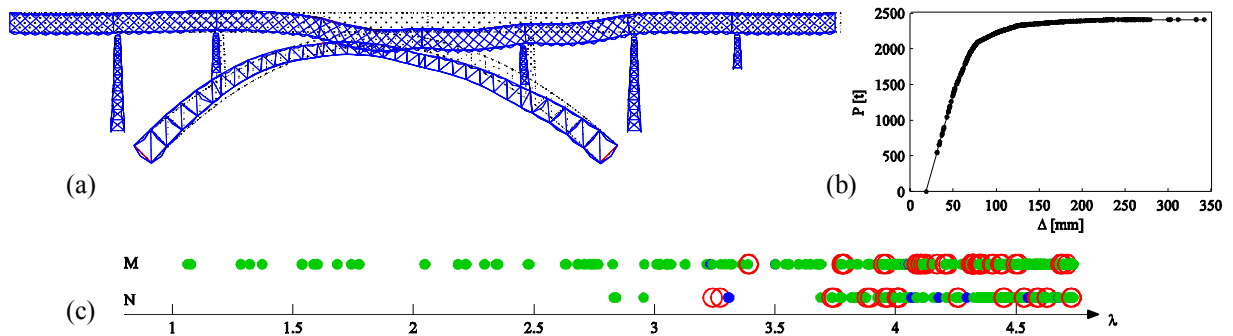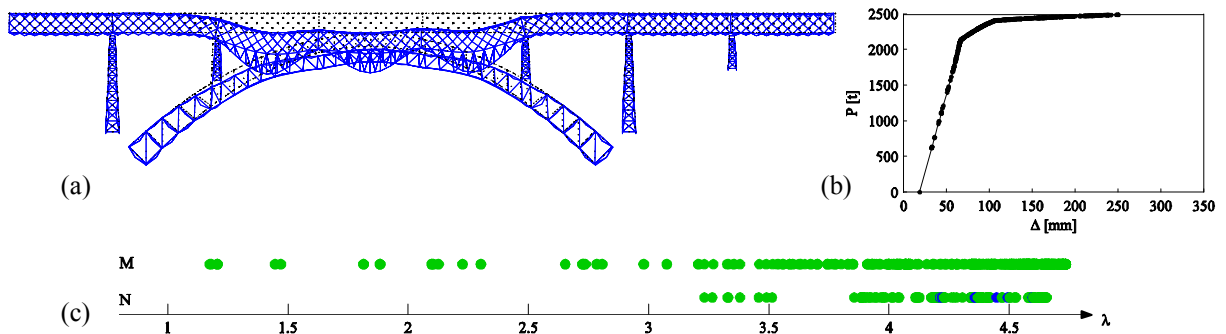

Fig. 4 Elastoplastic analysis of try-out Test I

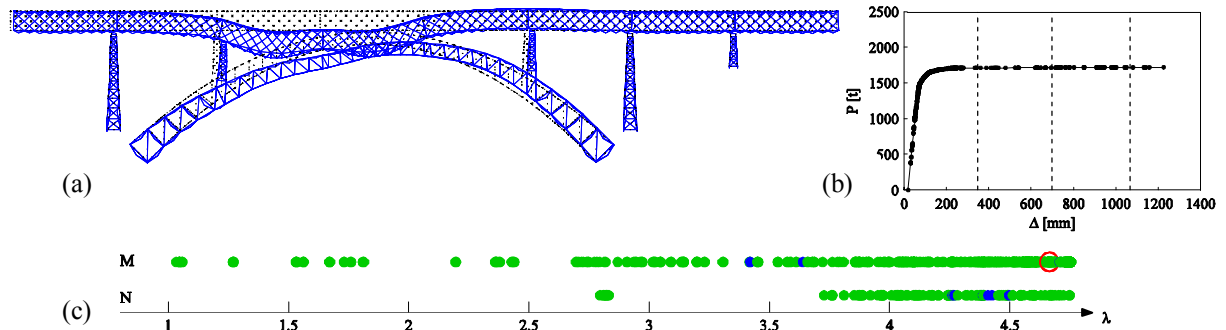**Fig. 5** Elastoplastic analysis of try-out Test II

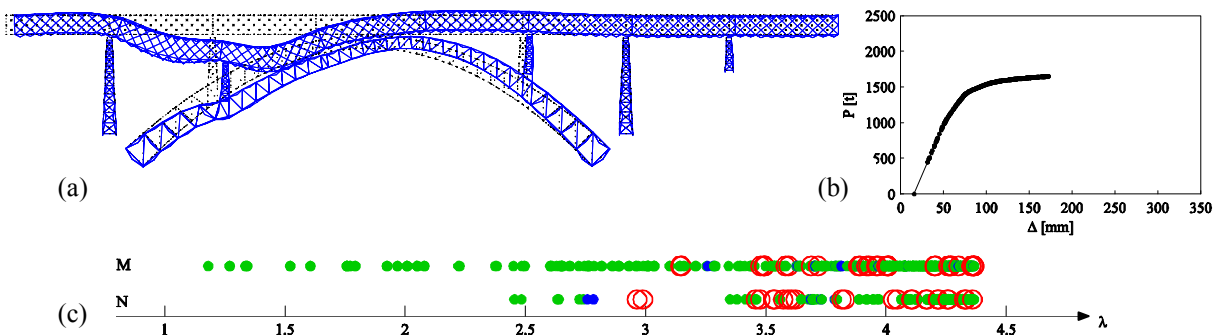**Fig. 6** Elastoplastic analysis of try-out Test III

Fig. 7 Elastoplastic analysis of try-out Test IV

should look reasonable for these vertical loading configurations that are symmetric to the longitudinal plane of the bridge. The colour of the markers refers to the various parts of the structure to which the activated plastic joint has appeared: to an element of the arch (blue), piers (red), upper continuous

2176

beam (green). In particular, the largest hollow circle marks a plastic mode activated in an element of the piers resting on the arch. So, in inspecting the maps reported in Figs. 4-7c, it is possible to appreciate the sequence of activation of plastic joints and the overall plastic response of the bridge, at increasing applied accidental load $P = \lambda\,Q$.

The load multipliers λ_c at incipient structural collapse of the bridge for the four loading configurations are reported in Table 1, with type and number of activated modes. Table 1 lists as well the maximum vertical node displacement of the bridge at incipient collapse (all maximum values refer to nodes of the upper continuous beam, at the railway level).

Table 1 Collapse load multiplier, active modes and maximum vertical displacement of the bridge

Load config.	$Q=nql$ [t]	Load mult. λ_c	$P_c = \lambda_c\,Q$ [t]	Nr. of active axial modes				Nr. of active flexural modes				Total nr. of active modes	Max vertical displ. [mm]
				Arch	Piers	Beam	Total	Arch	Piers	Beam	Total		
Test I	510	4.74	2417	8	16	112	136	14	12	91	117	253	343
Test II	510	4.73	2412	8	0	59	67	0	0	455	455	522	250
Test III	340	4.75	1615	6	0	96	102	3	2	525	530	632	1231
Test IV	340	4.37	1486	6	21	113	140	21	24	364	409	549	172

The obtained results show that, among the four tests (Fig. 3), the collapse load multipliers are almost the same, except for case IV (with two loaded spans), where the lower value $\lambda_c = 4.37$ is attained. This may be due to the fact that Test IV is the more eccentric with respect to the crown of the arch. In particular, the load is concentrated on the pier on the arch on the side of the Paderno d'Adda bank. As it can be appreciated in Table 1 and in Fig. 7c, this test presents the higher number of active modes in the piers (21 axial modes and 24 flexural modes). These modes are activated when the load multiplier reaches a value close to $\lambda = 2.4$ and seem then to rule collapse. Moreover, the maximum vertical displacement obtained at incipient collapse is, by far, the lowest. It may be said that, in Test IV, plastic collapse is reached without showing significant plastic resources in terms of global ductility. If the same total load is considered (in terms of resultant Q, Tests I-II and III-IV), but almost symmetrically distributed with respect to the crown of the arch, the collapse load multiplier obtained by the analysis increases (in particular, it becomes the highest in Test III).
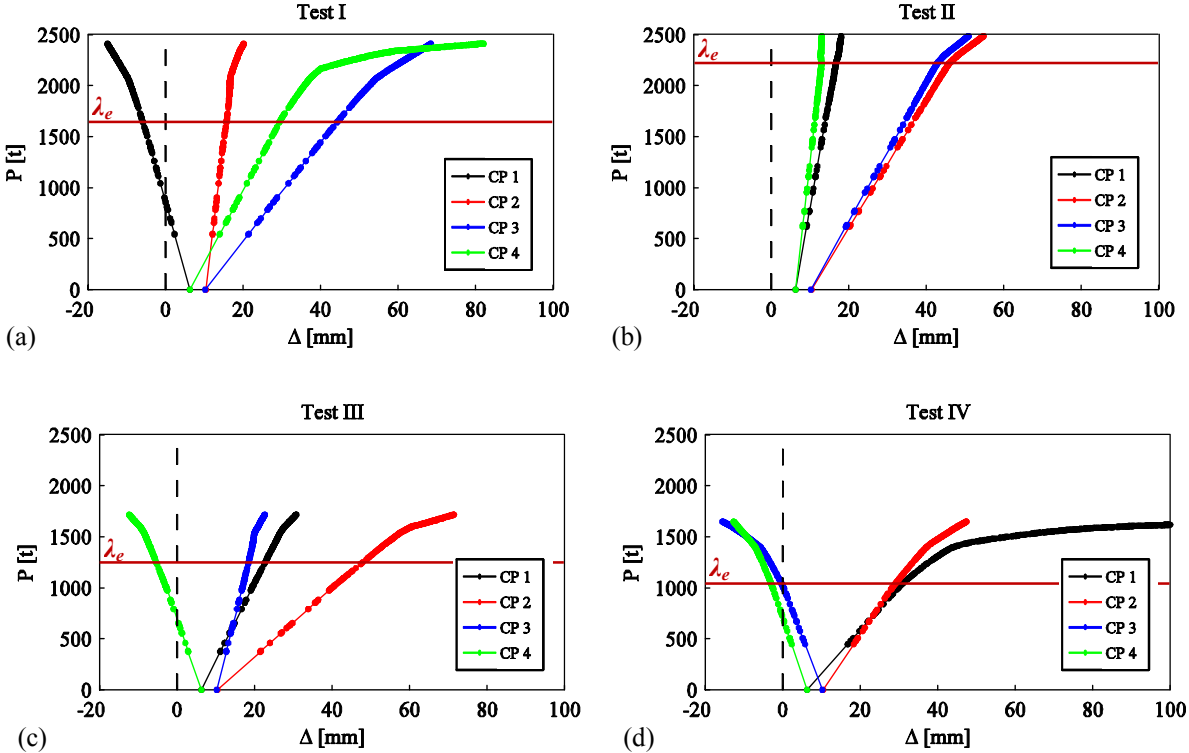

Fig. 8 Characteristic P-Δ curves at Control Points 1-4 (Fig. 3)

Fig. 6c for Test III shows that almost all yield modes activated at increasing load refer to the elements of the upper continuous beam; only few plastic modes are activated in the elements of arch and piers.

2177

The results obtained by the analysis referred to Test III show conspicuous plastic resources in terms of global structural ductility. In fact, as it can be appreciated in Fig. 6b, at incipient collapse, this loading configuration leads to a prolonged plateau and to the higher maximum vertical displacement (Table 1), up to about four times the maximum displacement in the other tests, which is referred to a node of the lower frame connecting the two main vertical longitudinal truss girders of the upper continuous beam, right underneath the rails, where the distributed load has been applied.

In Tests I and II three spans of the upper continuous beam are interested by the accidental load distribution. Despite this, in these tests the collapse load multiplier is not much different from those in Tests III and IV, so that the total collapse load P_c is higher. In Test I the total number of active modes is actually minimal and, near collapse, as in Test IV, many internal static variables in the elements of the piers do reach yield planes referred to both bending moments and axial force (Figs. 4c and 7c). In Test II many yield modes still refer to the elements of the upper continuous beam; no yield modes appear in the piers. The maximum vertical displacement obtained for Test II is quite limited (Fig. 5b, Table 1). Also in this case, collapse is reached without significant plastic deformations.

Fig. 8 below shows, for each of the loading tests (Fig. 3), the characteristic non-linear load/displacement response (P-Δ) curves at the four control points (CP 1-4) represented in Fig. 3. These are localised at the pier/beam and arch/beam interfaces, on the railway frame level and refer to the four bearings on the arch.

In Figs. 8a-d it is possible to note that, at selected CP_s, the collapse of the bridge is generally reached without significant plastic deformation at this level. Only in Tests I and IV (where the loads are much un-symmetrically located to the crown of the arch), Figs. 8a, 8d, plastic displacements are visible at CP 4 and CP 1, respectively. In Tests II and III the characteristic P-Δ curves stop quite early (global structural collapse of the bridge is achieved without appreciable vertical displacement at the CP_s). The P-Δ curves abandon the linear elastic trend at total load $P_e = \lambda_e Q$ (marked in Figs. 8a-8d by a horizontal line), scoring the threshold beyond which further loading generates permanent deformation in each of the tests (λ_e is in the order of 3.1 and 4.2 for Tests I and II, and in the order of 3.7 and 3.2 for Tests III and IV). The P-Δ trends are almost bi-linear, with visible kink right on the λ_e threshold (Test II) or a bit after that (Tests I, III and IV). The further post-kink load gain is quite limited, with respect also to threshold load (just a bit more visible for Test I). This seems to show that, for the considered loading configurations, the arch looks quite far from collapse, while structural collapse is reached for the bridge with reference to failure in the upper continuous beam and, in some cases, in some elements of the piers.

Instead, in all considered tests, the elements of the upper continuous beam appear to be the most critical within the structure. For each span of the beam, Fig. 9 below shows the location of the elements with activated plastic modes. Specifically, with counting of the number of activated modes, three couples of bars are displayed, on three levels, for each span of the beam: the top couple in the elements of the upper frame of the beam (thus at road level); the middle couple in the elements of the vertical frame of the longitudinal truss beams; the bottom couple in the lower frame (at railway level). Blue bars refer to axial modes and red bars to flexural modes. The width of the bars is related to the total number of active modes in the pertinent elements.
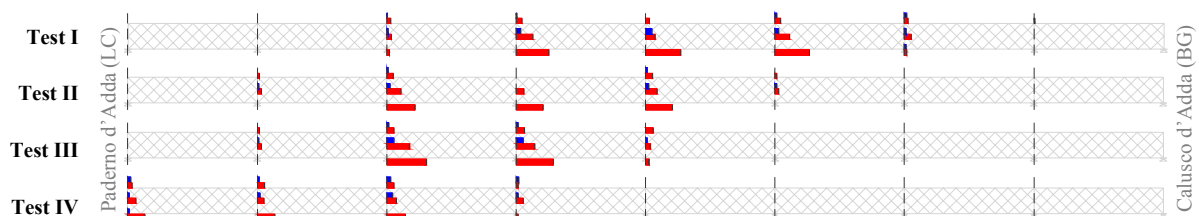

Fig. 9 Distribution of activated plastic modes in the upper continuous beam

Obviously, most active modes in the beam arise in the zones where the loads are applied, namely in the elements of the lower frame of the loaded spans. In Fig. 9 it is possible to appreciate that, for each loading configuration, these active modes are approximately one third of all the potential modes related to the lower frame; this ratio increases even more if (non activated) torsional modes are not taken into account and considering that very few elements do reach yield planes for the axial force. The number of active modes in the vertical and upper frames, of the same spans, does not appear negligible, with respect to that of the modes in the lower frame; some active modes arise also in

non-directly loaded contiguous spans. It may be said that loads applied at the railway level are able to involve the neighbouring elements in the plastic response of the continuous beam.

Notwithstanding that the plastic response of the structure in all tests appears to be governed mainly by the activation of the yield modes in the elements of the upper continuous beam, in Tests I and IV the modes referred to the elements of the piers directly lying on the arch are involved in the final collapse. No elements of the other piers yield. The analyses show that, in both Tests I and IV, the active modes in the piers on the arch refer to elements at the piers/arch connections and elements of the upper rectangular closing frame on top of the piers, hosting as well the bearing devices of the beam. No active modes arise in the elements of the four faces of the box profile of the piers.

4. CONCLUSIONS

In this paper, structural elastoplastic analyses of the Paderno d'Adda bridge (1889) have been performed. To this end, a dedicated computer program has been implemented, in which 3D beam finite elements, perfectly plastic joints (as an extension of classical plastic hinges), piece-wise linear yield domains and "exact" time integration (in the sense discussed in [15]) have been considered as main characteristic ingredients of the elastoplastic FEM formulation. The algorithm has shown very much able to track the limit structural behaviour of the bridge, through a sophisticated computational strategy, by reaching convergence with smooth runs up to the true limit load and corresponding collapse displacements. This holds true despite the considerable complexity of the complete bridge structure, involving roughly 5300 beam finite elements and 13300 degrees of freedom.

The obtained results, which refer to geometrical characteristics at design stage, show a good global elastoplastic performance of the bridge. Specifically, for the analysed loading conditions (with vertical loads acting symmetrically to the longitudinal plane of the bridge), the arch is basically never involved in the collapse. Actually, in all try-out tests only few elements of the arch yield. In this sense, it appears that the doubly-built-in parabolic arch, a marvellous characteristic feature of the bridge, represents a well-set structural element, in terms of the global structural response of the viaduct.

For all the analysed loading conditions, the elements of the upper continuous beam appear to be the most critical. It is worth-mentioning that, despite interventions on the roadway deck in the seventies and the more recent stiffening of the metallic box girder, the railway deck should not have undergone substantial modifications. Thus, further checks on the structural performance of the beam should be specifically pursued. The analyses have also shown that only tests with loading configurations much un-symmetrically located to the crown of the arch have involved plasticity in the elements of the piers, but right underneath the loaded spans, in particular at the arch/pier and pier/beam stiffened interfaces, where the FEM model is actually not that detailed so far (and could be refined), to deal appropriately with the stress concentrations that may produce at these locations. The other elements of the piers appear far from collapse. The structural members of the arch also appear rather in safe position, since they are hardly involved in the plastic sequence leading to collapse. The considerable level of load amplification at collapse (absolute λ_c in the order of 4.4-4.7, elastic λ_e in the order of 3.1-4.2 and multiplier ratio λ_c / λ_e in the order of 1.1-1.5) is certainly warranted by the assumed unlimited perfectly-plastic behaviour of all the structural members of the bridge, as linked to the stiff "hyperstatic" nature of the structure, as conceived at original design, which appears to allow for considerable stress transfer and redistribution at increasing load and resulting plastic deformation in the structure. Additional simulation loading settings, directly acting at the beam/piers or pier/arch interfaces may provide further information on the specific plastic resources of bearing structural subparts constituted by piers and arch.

The present preliminary results on the elastoplastic structural performance of the bridge have referred to design stage conditions. Further analyses could consider the current geometrical characteristics and state of conservation of the structure, which appears to be affected by diffused and localised corrosion damage, due also to lack of maintenance. While the present design-stage analyses seem to be rather encouraging about the bearing capacity of the bridge (under the assumption of unlimited ductility of the structural members), mainly regarding its vertical supporting structure made by arch and piers, degradation and aging may imply reduced structural performance. This should be checked in view of possible restoration actions, which appear worthwhile to be pursued, given the present results and the considerable importance and value that this historic infrastructure still keeps today in the local transportation network and in the architectural and industrial heritage of the territory.

ACKNOWLEDGEMENTS

REFERENCES

[1] Società Nazionale delle Officine di Savigliano (1889). Viadotto di Paderno sull'Adda (ferrovia Ponte S. Pietro-Seregno). *Tip. e Lit. Camilla e Bertolero, Torino.*

[2] Nascè V., Zorgno A.M., Bertolini C., Carbone V.I., Pistone G., Roccati R. (1984). Il ponte di Paderno: storia e struttura. Conservazione dell'architettura in ferro. *Restauro,* XIII (73-74).

[3] Ferrari R. (2006). Sulla concezione strutturale ottocentesca del ponte in ferro di Paderno d'Adda secondo la teoria dell'ellisse d'elasticità. *Laurea Thesis in Building Engineering*, Advisor E. Rizzi, Università di Bergamo, Facoltà di Ingegneria, I-24044 Dalmine (BG), Italy, 228 pages, December 2006.

[4] Ferrari R., Rizzi E. (2008). On the theory of the ellipse of elasticity as a natural discretisation method in the design of Paderno d'Adda Bridge (Italy), in *Proc. of 6th Int. Conf. on Structural Analysis of Historic Construction (SAHC08)*, D. D'Ayala and E. Fodde (Eds.), Bath, UK, 2-4 July, 2008, CRC Press, Taylor & Francis Group, Vol. 1, 583-591.

[5] Facheris M. (2009). Analisi morfologica e modellazione per elementi finiti della pila sull'arco del ponte di Paderno d'Adda. *Laurea Thesis in Building Engineering*, Advisor E. Rizzi, Co-Advisor R. Ferrari, Università di Bergamo, Facoltà di Ingegneria, I-24044 Dalmine (BG), Italy, 125 pages, September 2009.

[6] Ferrari R. (2009). Analisi strutturale degli elementi portanti del ponte di Paderno d'Adda. *Laurea (Master) Thesis in Building Engineering*, Advisor E. Rizzi, Università di Bergamo, Facoltà di Ingegneria, I-24044 Dalmine (BG), Italy, 108 pages, September 2009.

[7] Ferrari R., Facheris M., Rizzi E. (2010). Structural modelling of the piers of the Paderno d'Adda Bridge (1889, Italy), in *Proc. of 34th IABSE Int. Symposium on Bridge and Structural Engineering*, IABSE Reports, Vol. 97, Venice, Italy, 22-24 September 2010, Book of Abstracts, pp. 778–779; CD-ROM Proceedings, Paper A-634, 8 pages.

[8] Ferrari R., Facheris M., Rizzi E. (2010). Structural analysis of the Paderno d'Adda bridge (Italy, 1889), in *Proc. of 7th Int. Conf. on Structural Analysis of Historic Constructions (SAHC10)*, Eds. Xianglin Gu and Xiaobin Song, Shanghai, China, 6-8 October 2010, Advanced Materials Research, Vols. 133–134 (2010), 459-465.

[9] Ferrari R., Rizzi E. (2011). FEM modelling of the Paderno d'Adda bridge (Italy, 1889), in *Proc. of Structural Engineers World Congress (SEWC 2011)*, Como, Italy, 4-6 April 2011, Book of Abstracts p. 159; CD-ROM Proceedings, Paper 210, 9 pages.

[10] Ferrari R., Rizzi E. (2011). Analisi strutturale del ponte in ferro di Paderno d'Adda (1889), *Technical Report SdC2011/03 – June 2011*, Università degli Studi di Bergamo, Facoltà di Ingegneria (Dalmine), Dipartimento di Progettazione e Tecnologie, viale G. Marconi 5, I-24044 Dalmine (BG), Italy, 97 pages.

[11] Gentile C., Saisi A. (2010). Dynamic assessment of the iron bridge at Paderno d'Adda (1889), in *Proc. of 7th Int. Conf. on Structural Analysis of Historic Constructions (SAHC10)*, Eds. Xianglin Gu and Xiaobin Song, Shanghai, China, 6-8 October 2010, Advanced Materials Research, Vols. 133-134 (2010), 709-714.

[12] Gentile C., Saisi A. (2010). Dynamic monitoring of the Paderno iron arch bridge (1889), in *Proc. of 6th Int. Conf. on Arch Bridges (ARCH'10)*, Baochun Chen, Jiangang Wei (Eds.), Fuzhou, China, 11-13 October 2010, 22-37.

[13] Gentile C., Saisi A., Busatta F. (2011). Dynamic testing and permanent monitoring of an historic iron arch bridge, in *Proc. of 8th Int. Conf. on Structural Dynamics (EURODYN 2011)*, Eds. G. De Roeck, G. Degrande, G. Lombaert, G. Müller, Leuven, Belgium, 4-6 July 2011, Book of Abstracts p. 46; CD-ROM Proceedings, Paper MS07-243, 8 pages.

[14] Ferrari R., Cocchetti G., Rizzi E. (2012). Limit analysis of a historic iron arch bridge. Formulation and computational implementation. *Preprint*.

[15] Cocchetti G., Maier G. (2003). Elastic-plastic and limit-state analyses of frames with softening plastic-hinge models by mathematical programming, *Int. J. of Solids and Structures*, 40(25), 7219-7244.